# Functional sodium magnetic resonance imaging of the intact rat kidney

NIMROD MARIL, RAANAN MARGALIT, JOEL MISPELTER, and HADASSA DEGANI

*Department of Biological Regulation, Weizmann Institute of Science, Rehovot, Israel; and Institut Curie, Centre Universitaire d'Orsay, France*

**Functional sodium magnetic resonance imaging of the intact rat kidney.**

*Background.* Renal fluid homeostasis depends to a large extent on the sodium concentration gradient along the corticomedullary axis. The spatial distribution and extent of this gradient were previously determined by invasive methods, which yielded a range of results. We demonstrate here the capacity of sodium magnetic resonance imaging (MRI) to quantify noninvasively renal sodium distribution in the intact kidney.

*Methods.* Sodium MRI was applied to study normal, diuretic, and obstructed rat kidneys in vivo. The images were recorded at 4.7 Tesla using a 3-dimensional gradient echo sequence, with high spatial and temporal resolution. The tissue sodium concentration (TSC) was obtained by taking into account the measured nuclear relaxation rates and MRI visibility relative to a reference saline solution.

*Results.* The corticomedullary sodium gradient increased linearly from the cortex to the inner medulla by $\sim$31 mmol/L/mm, from a TSC of $\sim$60 mmol/L to $\sim$360 mmol/L. Furosemide induced a 50% reduction in the inner-medulla sodium and a 25% increase in the cortical sodium. The kinetics of these changes was related to the specific site and mechanism of the loop diuretic. Distinct profiles of the sodium gradient were observed in acute obstructed kidneys, as well as spontaneously obstructed kidneys. The changes in the sodium gradient correlated with the extent of damage and the residual function of the kidneys.

*Conclusion.* Quantitative assessment of the renal corticomedullary sodium gradient by high resolution sodium MRI may help verify new aspects of the kidney concentrating mechanism and serve as a non-invasive diagnostic method of renal function.

The urinary concentrating process is associated with the generation of a corticomedullary osmolality gradient of sodium and urea in the medullary tissue, which is essential for fluid homestasis. Thus far, the characterization of the sodium gradient along the corticomedullary axis, as well as of induced changes in the gradient profile [1, 2], were based on invasive methods such as micropuncture [3, 4], radioautographic [5], and slice-section analytic procedures [6–8]. These studies yielded diverse results with either linear or exponential sodium increase in the inner medulla. As theoretical models of the kidney concentrating mechanisms rely on these measurements ([9–11] and references cited therein), it is important to quantify these gradients in the intact kidney, under controlled physiologic conditions. Sodium magnetic resonance imaging (MRI) provides the unique ability to directly measure and determine the tissue sodium concentration non-invasively [12–16]. Furthermore, since renal sodium distribution is tightly associated with its function, this imaging technique can serve to monitor renal function. Remarkably, although the kidney is the most obvious candidate organ for sodium imaging, there are only a few preliminary sodium MRI studies of this organ. A capability to delineate the kidney through its high sodium was shown by imaging the abdomen of guinea pigs [17] and humans [18]. Sodium spectra of the exposed rat kidney, recorded using the rotating frame method, revealed the highest level of sodium in the outer medulla and not, as expected, in the inner medulla [19]. Other studies that detected the corticomedullary sodium gradient were performed on the exposed rabbit kidneys [20–22]; hence, stress and unstable conditions could prohibit accurate characterization of renal sodium. Moreover, in these preliminary studies the sodium gradient was not quantified in terms of content or concentration units.

In this study we present a non-invasive in vivo investigation of sodium distribution in the intact rat kidney by means of high-resolution sodium MRI. We further show for the first time the capability of this methodology to quantify the sodium gradient and follow temporal and spatial changes during loop diuresis, as well as diseased states. Hence, this sodium MRI can provide a powerful non-invasive tool for diagnosing and assessing renal function.

## METHODS

### Animals and procedures

The study was performed on female adult Lewis rats (250–300 g) fed a standard chow diet and allowed tap water ad libitum. In experiments with control, normal kidneys the rats were allowed free access to the water. In experiments with control, antidiuretic rats water was withdrawn 24 hours prior to each experiment. The rats were anesthetized by an intraperitoneal injection of sodium pentobarbital at a dose of 0.04 mg/g wt.

Diuresis was induced by a bolus injection of a furosemide solution of 10 mg/mL (Hoechst, Frankfurt, Germany) into the rat-tail vein, at a dose of 10 mg/kg/wt. Urine samples from untreated normal rats, antidiuretic rats (24-hour water withdrawal), and from diuretic rats were collected in a metabolic cage, starting 15 minutes after the injection of the vehicle or furosemide. Urine sodium concentration in each sample was determined by sodium nuclear magnetic resonance (NMR) measurements using a Bruker DMX-400 spectrometer (Bruker, Rheinstetten, Germany) at 106 MHz, with 90° pulses, pulse-to-acquisition delay of 6 μs, repetition time of 0.74 seconds, and acquiring 10 scans. The urine was transferred after centrifugation (for 10 minutes, 10,000$g$, at room temperature) to a 5-mm NMR tube placed concentrically in a 10-mm NMR tube that contained a reference solution of 120 mmol/L NaCl and 5 mm of the sodium shift reagent thulium (III) 1,4,7,10-tetraacyclododecane-1,4,7,10-tetrakis (methylene phosphonate) (TmDOTP$^{5-}$) (Macrocyclics, Dallas, TX, USA). Each sodium spectrum exhibited a signal due to the urine sodium and a signal due to sodium in the reference solution that was shifted by ∼8 ppm (not shown). Analysis of the $^{23}$Na spectra was performed with an XWIN-NMR Bruker software package. Sodium concentration in the urine was calculated from the integrated area of its signal, referenced to the integrated area of shifted signal of the sodium in the reference solution.

Acute obstruction was induced by ligations of the ureter near the pelvic-ureter junction with a double 5/0 silk suture. The sodium images were recorded 48 hours after the ligation. The extent of damage was assessed by inspecting histopathologic specimens of the kidneys, stained by hematoxylin-eosin, which were dissected out and fixed after the MRI experiment. We also measured the creatinine levels in the plasma of the rats 2 days after the obstruction. Blood was obtained from anesthetized rats by retro-orbital sinus puncture, and collected in a tube containing 100 μL heparin (Elkins-Sinns, Inc., Cherry Hill, NJ, USA). Following centrifugation at room temperature for 10 minutes (10,000$g$), the supernatant was separated and creatinine level was determined spectrophotometrically (500 nm) using a standard creatinine kit (Sigma Diagnostics, Inc., St. Louis, MO, USA).

Spontaneous obstruction was diagnosed in two rats by contrast-enhanced MRI [23] and was reconfirmed by an analysis of the hematoxylin-eosin stained histologic specimens of these kidneys.

All of the animal protocols and maintenance were in accord with the guidelines of the Committee on Animals of the Weizmann Institute of Science and were approved by this committee.

### In vivo MRI

Proton and sodium images were recorded at 200 and 53 MHz, respectively, with a 4.7 T Biospec spectrometer (Bruker, Rheinstetten, Germany) using a home built 3-cm, double-tuned $^1$H and $^{23}$Na surface coil. Calibration of this coil confirmed B1 field homogeneity within the coil in planes parallel to its surface and mapped the change in B1 as a function of the vertical distance from the center of the coil. The rats were placed in a supine position with the kidney positioned in the middle of the coil. Localization of the kidney in the center of the coil was adjusted by recording fast 3-D $^1$H gradient echo images using the same field of view as in the sodium images. Three-dimensional $^{23}$Na gradient echo images were recorded using (TE/TR) of 1.7/60 ms, a 90° sine/cosine adiabatic pulse [24], field of view (FOV) of 12 × 12 × 4.8 cm, and a matrix of 128 × 128 × 16, accumulating 10 scans (total scanning time of 20 minutes). The third dimension (projection thickness) and the angle of the FOV were carefully chosen in order to minimize partial volume effects. Delineation of the kidney boundary as well as regions of interest (ROI) was performed using the $^1$H images recorded with the same spatial resolution as that of the $^{23}$Na images. Changes in signal intensity were normalized in reference to the signal intensity in the start of the cortex (relative intensity units). Signal intensity was enhanced by applying a Fermi filter before the Fourier transformation. The relative intensities in the filtered images remained the same as in the original images by selecting the appropriate parameters of the Fermi filter. Fast sodium imaging with a temporal resolution of 4 minutes was achieved by increasing the FOV to 16 × 16 × 8 cm and accumulating 2 scans. Image analysis accounted for the inhomogeneity in the radio frequency pulse strength, using field profiles measured for a phantom sodium solution. Measurements of the sodium longitudinal ($T_1$) and transverse ($T_2$) relaxation rates of excised kidneys, as well as in vivo, indicated similar rates in the cortex and the medulla. Hence, the changes in signal intensity along the corticomedullary axis were directly proportional to changes in tissue sodium concentration (TSC). The sodium visibility [25] was calculated by referencing the signal intensity in the kidney to that of a standard saline solution placed in a sealed tube (4 mm diameter), which was implanted near the left kidney of three rats two days prior to the MRI experiment. This enabled us to calculate the TSC

according to [12–14, 26]:

$$TSC = \frac{S^{tiss} \times [Na]^{std}}{S^{std}} \times \frac{1 - \exp(-TR/T_1^{std})}{1 - \exp(-TR/T_1^{tiss})}$$

$$\times \frac{\exp(-TE/T_1^{std})}{0.6 \times \exp(-TR/T_{2f}^{tiss}) + 0.4 \times \exp(-TE/T_{2s}^{tiss})}$$

where S is the signal intensity, "std" and "tiss" designate the standard saline reference and the tissue, respectively. The measured fast and the slow $T_2$ relaxation times were: $T_{2f}^{tiss} = 2.2$ ms and $T_{2s}^{tiss} = 20.4$ ms, respectively, and $T_1^{tiss} = 34$ ms. The relaxation times of the standard saline reference were $T_1^{std} = T_2^{std} = 60$ ms [27].

## RESULTS

### The sodium gradient in the normal kidney

High-resolution sodium images of the rat kidney demonstrated increased sodium content in this organ relative to the surrounding tissues (Fig. 1A). The corresponding proton images confirmed the localization of the kidney at the center of the radio frequency surface coil (Fig. 1B). Due to both the higher nuclear magnetic resonance sensitivity of a proton relative to that of a sodium nucleus (~one order of magnitude) and the higher tissue proton concentration relative to that of sodium (~two orders of magnitude), the signal to noise ratio in the proton images was markedly higher. Recording sequentially coronal sodium images of the same kidney showed a constant sodium distribution and stable sodium gradient over time. The sodium signal intensity appeared to increase gradually along the corticomedullary axis from the edge of the cortex through the outer and the inner medulla (Fig. 1C). It should be noted that the sodium intensity in the papilla tip was reduced due to partial volume effects in this location.

Pixel-by-pixel analysis of the sodium signal intensity along the corticomedullary axis enabled us to quantify the gradient (Fig. 1D). The gradual increase in normal kidneys exhibited a good linear fit ($R = 0.97 \pm 0.01$; $N = 20$), with a slope of $0.51 \pm 0.03$ in relative intensity units per mm (normalized to 1 in the start of the cortex). A similar linear increase with a slope of $0.53 \pm 0.12$ in relative intensity units per mm ($N = 3$) was obtained in normal kidneys of rats maintained under antidiuretic conditions (24 hours of water withdrawal) prior to the experiments. We cannot exclude, however, the presence of local deviations from linearity at a higher spatial resolution or due to some partial volume effects, particularly at both edges. The conversion of the intensity units to tissue sodium concentration units (see **Methods**) yielded a slope of $31 \pm 3$ mmol/L/mm, from ~60 mmol/L in the start of the cortex to ~360 mmol/L in the inner medulla edge.
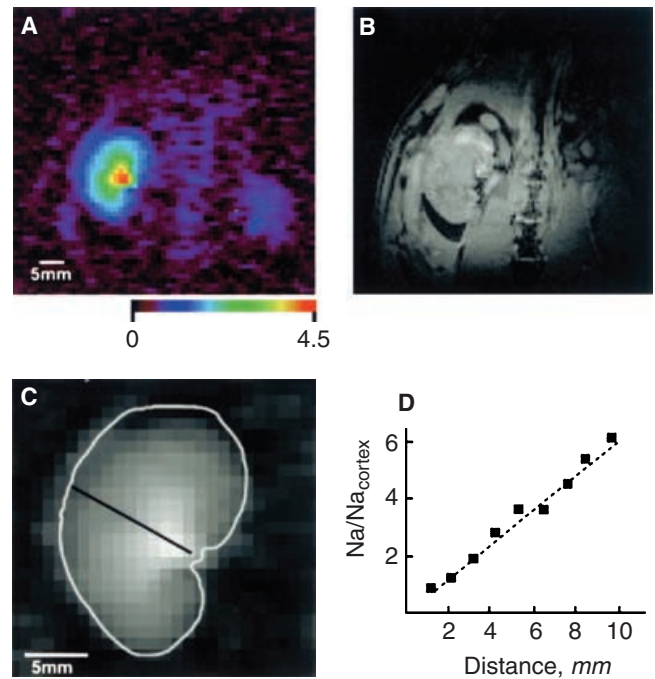


**Fig. 1. Magnetic resonance imaging (MRI) of the sodium gradient in the rat kidney.** (*A*) A coronal projection of a 3-D $^{23}$Na image of the right intact kidney of a control rat. The image demonstrates the distribution of the sodium signal in the kidney and in the surrounding environment. (*B*) A coronal projection of a 3-D $^1$H image of the same region as in (A). The image shows the localization of the kidney in the center of the surface coil and the presence of the adjacent organs. (*C*) Enlargement of the region of the kidney in (A) to emphasize the gradual change in signal intensity from the cortex to the inner medulla along the corticomedullary axis (black line). The kidney is delineated by a white boundary defined in the corresponding proton image. (*D*) The increase in sodium content along the corticomedullary axis. Sodium signal intensities were measured at pixel resolution and referenced to the signal intensity at the start of the cortex. The $^{23}$Na and $^1$H images were recorded using a 3-D gradient echo sequence with a field of view of 12 × 12 × 4.8 cm. The $^{23}$Na image was acquired with TE/TR of 1.7/60 milliseconds, matrix of 128 × 128 × 16 and 10 scans (20-minute scanning time). The $^1$H image was acquired with TE/TR of 6/30 milliseconds, matrix of 256 × 256 × 32, and 1 scan (2-minute scanning time).

### The sodium gradient in diuresis

The capacity of the sodium images to reveal functional changes due to physiologic perturbations were exhibited by monitoring diuresis at high temporal resolution. Images recorded at high temporal resolution (each either 2 or 4 minutes) before and sequentially after the administration of the loop diuretic furosemide revealed marked changes in the sodium gradient. The effect was dominated by a marked exponential decrease in the inner medulla sodium, by $44 \pm 6\%$, with a characteristic decay constant of $6.1 \pm 0.8$ minutes (Fig. 2A). In parallel, a smaller and slower sodium exponential increase was observed in the cortex, of $27 \pm 1\%$, and with a time constant of $9 \pm 1$ minutes, respectively (Fig. 2B, $N = 7$).

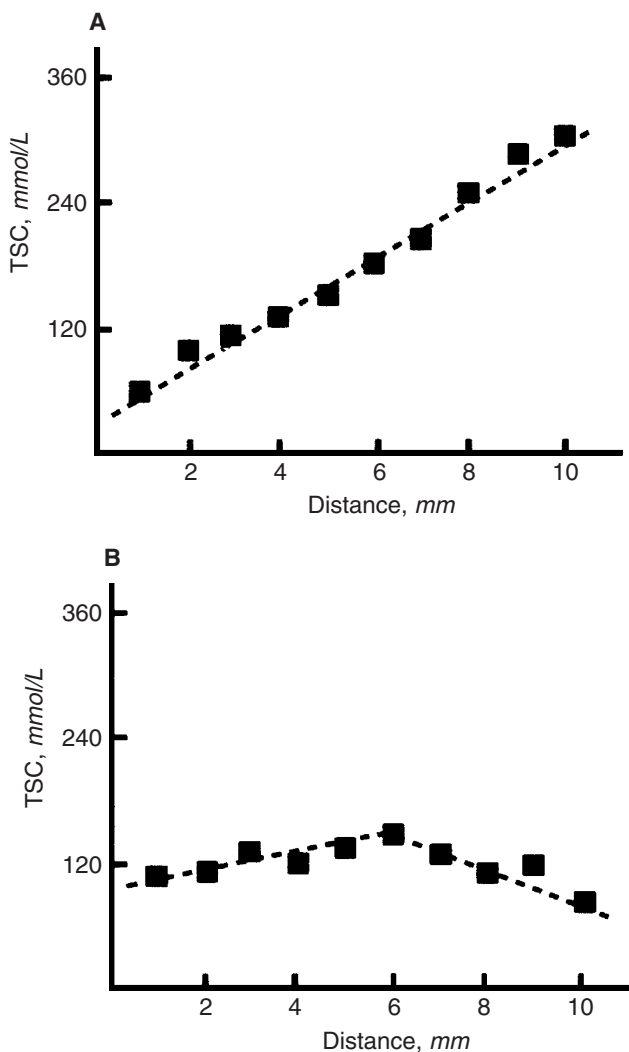Fifteen minutes after furosemide administration a condition of steady-state diuresis was established for more
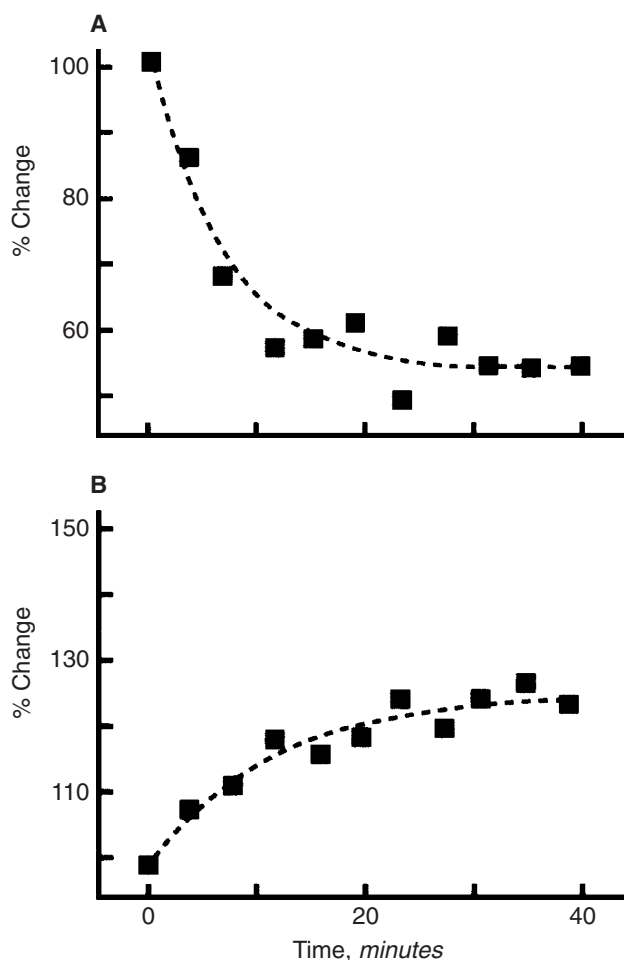
**Fig. 2. Typical kinetics of the regional changes in renal sodium during furosemide-induced diuresis.** Time courses of sodium signal intensity relative to that before administration of furosemide (in percentage) in the inner medulla (*A*) and cortex (*B*). Data were obtained by means of an ROI-based analysis of sequential sodium images (temporal resolution 4 minutes) recorded prior to and immediately after a bolus injection of furosemide (10 mg/kg wt), as described in **Methods**.



**Fig. 3. Renal tissue sodium concentration along the corticomedullary axis at steady-state control (*A*) and steady-state diuresis (*B*).** Sodium signal intensity was measured in the same kidney before and 15 minutes after administration of furosemide (10 mg/kg wt). Intensity units at pixel resolution were converted to tissue sodium concentration units as described in **Methods**.

than 40 minutes, with the sodium gradient almost completely cancelled (Fig. 3). This cancellation correlated with an expected increase in the concentration of the sodium in the urine [28, 29], measured by means of $^{23}Na$ NMR spectroscopy; urine sodium concentration in rats under furosemide steady-state diuresis was 135 ± 5 mmol/L (*N* = 3), whereas in control rats with free access to water it was 90 ± 6 mmol/L (*N* = 3). The highest TSC during steady-state diuresis was localized in the outer medulla, with the cortex to outer medulla slope of sodium signal intensity reduced by ~fivefold. Due to the large sodium decrease in the inner medulla the outer to inner medulla slope became slightly negative (*N* = 7).

## The sodium gradient in the obstructed kidney

Sodium MRI enabled us to assess specific pathologic changes due to acute, as well as unprompted, natural ob-

struction of the ureter. $^{1}H$ MR imaging of the acutely obstructed kidneys indicated an increase in volume of ~30%. The sodium distribution in these kidneys (*N* = 5) was very different from that of the normal kidneys (Fig. 4A). Macro inspection of the histologic specimens of the acutely obstructed kidneys revealed a marked reduction in the parenchyma thickness (corticomedullay length of 4 ± 1 mm compared to ~12 mm in the normal kidney, *N* = 7), with the atrophy of the perihelia region larger than that of the circumference, resulting in a flattened inner medulla (Fig. 4B). Pixel-by-pixel analysis of the sodium images along the corticomedullary axis indicated a significant decrease of ~ twofold in the cortico- to outer-medulla sodium gradient (to 0.23 ± 0.04 in relative intensity units per mm) in reference to that of normal kidneys
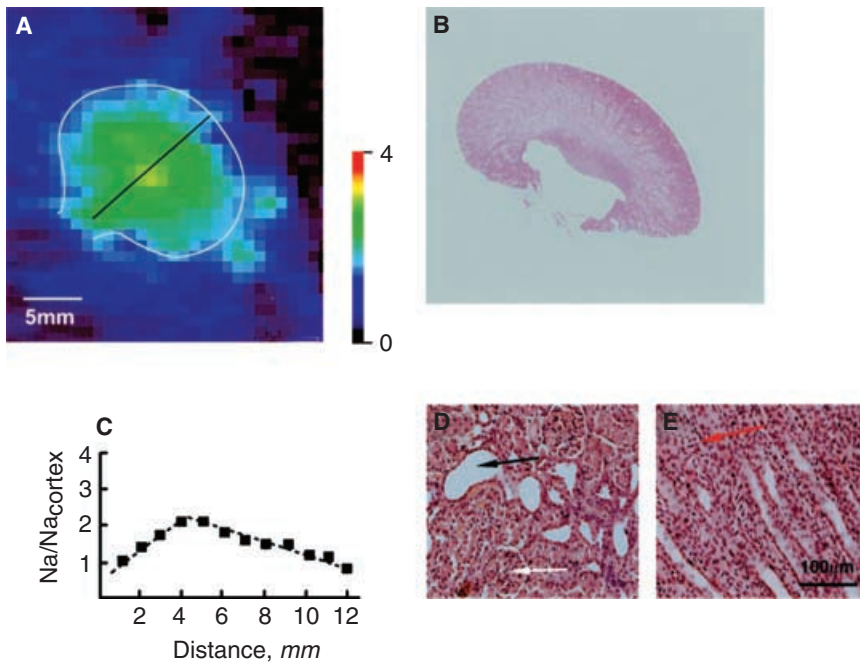
**Fig. 4. Renal sodium distribution under conditions of acute hydronephrosis.** (*A*) A typical sodium image of the obstructed kidney. (*B*) A macro picture of a histologic slice of the imaged kidney showing the extent of the residual parenchyma. The orientation of the kidney in the sodium image is similar to that of the histologic slice. (*C*) A typical profile of the corticomedullary sodium gradient induced by acute hydronephrosis. (*D* and *E*) Microscopic views of hematoxylin-eosin stained sections of renal cortex and medulla, respectively. The acute hydronephrotic kidney shows marked dilation (black arrow) and tubular damage (gray arrow) and glomerular atrophy (white arrow).The image was recorded using a 3-D gradient echo sequence using the same recording parameters as in Figure. 1. The kidney is delineated by a white boundary defined in the corresponding proton image.
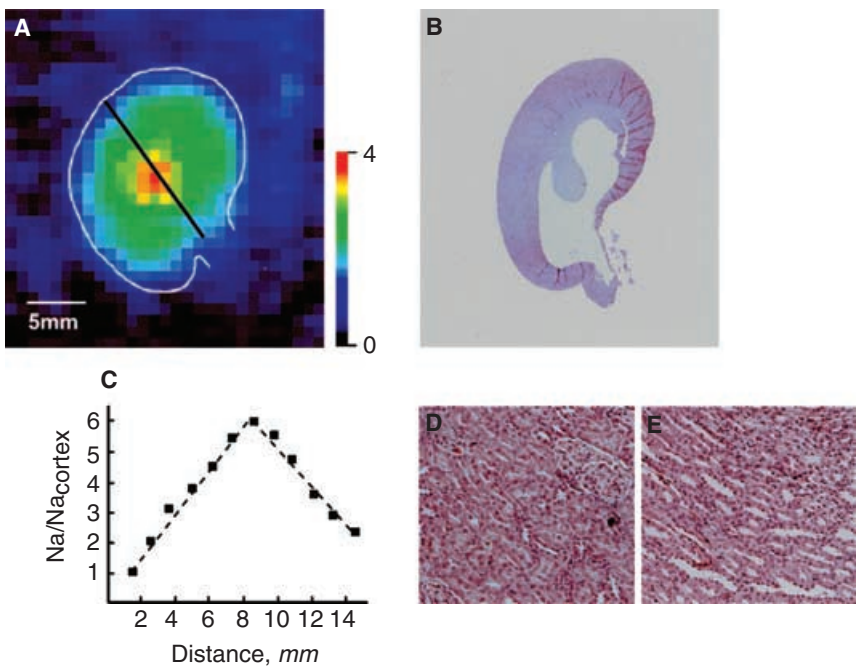


**Fig. 5. Renal sodium distribution under conditions of spontaneous hydronephrosis.** (*A*) A typical sodium image of the obstructed kidney. (*B*) A macro picture of a histologic slice of the imaged kidney showing the extent of the residual parenchyma. The orientations of the kidney in the sodium image are similar to that of the histologic slice. (*C*) A typical profile of the corticomedullary sodium gradient in the spontaneously developed hydronephrotic kidney. (*D* and *E*) Microscopic views of hematoxylin-eosin stained sections of renal cortex and medulla, respectively. The spontaneous hydronephrotic kidney shows normal glomeruli and tubules. The image was recorded and presented as described in Figure 4.

(Fig. 4C). Moreover, the sodium gradient from the outer medulla toward the papilla tip was substantially reduced. The microscopic inspection of the acutely obstructed kidneys indicated a vast cortical and medullar tubular dilation, stenosis, and atrophy (Fig. 4D and E). Despite of all the aforementioned changes, evaluation of the kidney function by the level of creatinine in the plasma showed no significant difference between acute hydronephrotic rats, $0.61 \pm 0.04$ mg/dL, ($N = 5$) and control rats, $0.54 \pm 0.03$ mg/dL ($N = 10$). This suggested that the function of the second healthy kidney remained sufficient to compensate for the damaged kidney; however, the sodium image could clearly depict changes due to unilateral hydronephrosis.

The sodium images of the kidneys of rats that developed spontaneously unilateral hydronephrosis exhibited an abnormal sodium distribution (Fig. 5). The deviation from a normal sodium gradient was different, however, from that observed in acute hydronephrotic kidneys (Fig. 4). Histologic specimens of the obstructed

kidneys confirmed hydronephrosis (Fig. 5B). However, the kidneys maintained an extended elongated inner medulla relative to that observed in the acute obstructed kidneys. In the sodium image of these kidneys the highest sodium signal was confined to a location in the middle of the kidney that was seen in the proton image at the end of the parenchyma. The sodium gradient from the cortex toward this location (Fig. 5C) was similar to the maximal gradient in control kidneys. However, the obstruction reduced the sodium content in the dilated inner region of the kidney (Fig. 5A and C). Microscopic inspection of the histologic specimens showed that the structure and cellular morphology of the remaining kidney tissue appeared unharmed, with no glomerular or tubular stenosis, necrosis, or atrophy (Fig. 5D and E). Thus, despite the distortion in the distribution of the sodium due to the hydronephrosis, the sodium gradient in the remaining regions of these kidneys was fully maintained; hence, the region of residual renal function could be localized.

## DISCUSSION

The mechanism by which the kidney can conserve water while maintaining excretion of solutes is achieved by the countercurrent multiplication in the renal medulla. The effect in the outer medulla is known to be primarily due to the active NaCl reabsorption in the thick ascending limb [30]; however, the inner medullary osmolarity gradient has still not been adequately explained [10, 11, 31]. Continued experimental studies that quantify the extent and spatial distribution of solute gradients in great detail may therefore help to fully clarify the mechanism of urinary concentration. Indeed, the application described here of sodium MRI provided a unique means to determine non-invasively and reproducibly the spatial and temporal changes in renal sodium distribution of the intact organ. The sodium images of the normal kidneys revealed a gradual increase in the sodium signal intensity from the cortex toward the edge of the inner medulla. With the current spatial resolution along the corticomedullary axis (0.9 mm), this increase appeared linear. The signal intensities were converted to tissue sodium concentrations, which provided an average measure of sodium content per voxel. This conversion was previously demonstrated in other organs and was shown to yield TSC values, which were verified by classic methods [12–14, 26]. The renal TSC increased linearly from 60 mmol/L in the cortex boundary to 360 mmol/L at the inner medulla edge. These values are within the range of concentrations reported using a slice sectioning method that measured the total amount of sodium in each slice [6–8, 32–35]. Lower values of TSC (25–40 mmol/L) were reported in other organs, such as human calf muscle [15, 16], rat brain [12], and perfused dog heart [13].

The relatively high TSC value in the renal cortex predominantly reflected the high extracellular volume fraction (including the intratubular space) in the cortex, as compared to that in the other organs. A similar value of TSC was reported for focal cerebral tumors, which also contain a relative high extracellular volume fraction [14]. Based on previous results ([36] and references cited therein) that showed a sodium concentration in the cortical extracellular space similar to that in blood plasma, we estimated from our measurements (TSC of 60 mmol/L) an extracellular volume fraction of ~40% in this region. This value is in accord with results obtained in cortical slices of 30% to 50% [37, 38].

The medullary hypertonicity, however, was shown to be due to solute accumulation in the interstitium as well as in other medullary structures, including loops of Henle, vasculature, and collecting ducts [11, 39]. The extent of hypertonicity in the different tissue compartments could vary. The tissue sodium concentration that measures the average sodium content per voxel depends, therefore, on the sodium osmolarity in each of the above-mentioned compartments and on its corresponding volume fraction. Hence, the increase in the TSC in the outer and inner medulla reflected both an actual increase in sodium concentration and an increase in tissue volume fractions containing high sodium concentrations [37].

Although the MRI results of averaged TSC values cannot relate directly to model calculations, it can help assess ratios derived from model calculations. The maximal ratio of tissue sodium concentration in the inner medulla relative to the cortex edge was about 6:1, and that in the inner medulla relative to the corticomedullary junction of about 3:1. Calculation of the average TSC in each region of the kidney (the cortex, outer and inner medulla) yielded a ratio of 4:1 between the inner medulla and the cortex. These ratios are within the range of values found in previous studies using a variety of invasive methods [3, 4, 8, 22, 32, 34, 40–43].

Since the introduction of the countercurrent multiplication hypothesis in 1951 by Harrgitary and Kuhn [44], numerous additional models were suggested ([9–11] and references cited therein) and experimental data were obtained to support the models [5, 39–41, 45]. A recent model of volume and solute microvascular exchange in the renal medulla was extended by simulating the deposition of NaCl, urea, and water into the medullary interstitium from the loops of Henle and collecting ducts, with generation rates that undergo spatial variation within the inner medullary interstitium [10]. This study indicated a similar sodium (and urea) concentration in the ascending and descending vasa recta, as well as in the medullary interstitium. It also predicted that sodium might increase linearly or exponentially, depending on whether the increase in the interstitial area-weighted

generation rate of sodium ion increases linearly or exponentially, respectively. Although an exponential increase was observed by Koepsell et al [41], other results [5, 39, 40, 45] support a linear-like increase, and our observation demonstrated a linear increase in TSC in kidneys under normal and antidiuretic conditions. An exponential increase in the inner medulla sodium concentration will require a large decrease in the fraction of regions with high sodium. Hence, the MRI results appear to be in accord with the model that applies a linear interstitial area–weighted generation rate of the sodium ions. The ratio of TSC in the inner medulla to that in the corticomedullary junction obtained in our study, ($\sim$3) was close to that predicted by the model for the linear increase (of about 2.6), [10] as well as to the prediction by Wang et al [9] and by Thomas [46]. This ratio was not affected by increasing antidiuretic conditions (water withdrawal for 24 hours), as was also indicated by the results of Koepsell et al [41], which showed a several-fold higher ratio, but no correlation between this ratio and the degree of antidiuresis. It should be noted that a large ratio was recently calculated by introducing inner medullary lactate production as an additional mechanism for urine concentration in the inner medulla [31]. Thus, although other parameters calculated by the theoretical models need to be tested experimentally as well (i.e., urine gradient), the detailed analysis of the sodium content in the intact kidney adds a new tool for validating proposed models. Further advancement in the MRI technology will help increase the spatial resolution and improve defining sodium compartmentation.

The capacity of sodium MRI to monitor changes in the renal sodium gradient can enhance our understanding of the action of drugs and particularly help diagnose the development of renal diseases. The change in the sodium gradient during diuresis served to illustrate the physiologic implications of sodium MRI, and diuretics have been also used to clarify the mechanism of the kidney concentrating function [47].

Loop diuretics, such as furosemide, directly inhibit the $Na^+/2Cl^-/K^+$ cotransporter present in the luminal membrane of the medullar thick ascending limb, reducing the absorption of sodium and chloride ions [48]. Consequently, the countercurrent mechanism becomes inoperable, eliminating sodium reabsorption into the interstitium and reducing the sodium gradient. Indeed, we observed both the temporal changes and the final drastic reduction in the corticomedullary sodium gradient induced by furosemide. The time course of the effect of furosemide on the outer to inner-medulla sodium gradient reflected, most likely, the time it took this drug to reach its site of activity in the apical membrane of the thick ascending limb [49]. Furosemide, as all other loop diuretics, is bound tightly to serum proteins and, there-

fore, when it is delivered to the glomerulus it is not filtered. The protein-bound furosemide reaches, therefore, in this state the postglomerular circulation, where it dissociates and is secreted into the tubular lumen by an anion transporter [50].

The loop diuretics also inhibit $Na^+$ and $Cl^-$ absorption by macula densa cells [47]. Therefore, loop diuretics abolish the tubuloglomerular feedback, which prevents sodium losses, and maintain the glomerular filtration rate high, despite the increase in the distal sodium and chloride ions [51]. The small, but persistent increase in the cortical sodium by furosemide, concomitant to its effect on the medullar gradient, appears therefore to reflect higher load of sodium in the cortical distal tubule, together with the loss of tubuloglomerular feedback and the enhanced glomerular filtration rate. Verification of this observation may be useful for identifying mediators of the tubular glomerular feedback.

Finally, we also demonstrated here the diagnostic capacity of renal sodium MRI by monitoring changes in acute and spontaneously obstructed kidneys. Obstructive uropathy caused by urethra obstruction is one of the most common diseases of the urinary tract. The most commonly employed techniques to diagnose the obstructive pathology of the urinary tract are urography and sonography [52–54]. Dynamic contrast–enhanced MRI can also reveal the presence of obstruction in the kidney ([55] and references cited therein). However, this method provided limited information about the residual function of the obstructed kidney. On the other hand, sodium imaging could clearly identify the regions that maintained residual function, as well as assess the extent of functionality.

In both acute and spontaneous hydronephrosis, the corticomedullary sodium gradient was altered. A marked reduction was observed in the inner medulla sodium level, which correlated with the vast parenchyma atrophy and the changes observed in the corresponding histologic slides. The clear tubular damage observed in the acute, and not in the spontaneous, hydronephrotic kidneys correlated with the marked decrease in the sodium gradient. On the other hand, the gradient was conserved in regions of the spontaneously obstructed kidneys that remained almost intact. In addition, the extended inner medulla, observed in the spontaneously obstructed kidneys, was also in accord with the preserved sodium gradient in these kidneys, in contrast to the acute hydronephrotic kidneys, which exhibited a flattened inner medulla. Hence, on the basis of the sodium images it was possible to distinguish between partial and complete obstruction and non-invasively assess the residual functions of the partially obstructed kidneys. Sodium MRI can, therefore, be applied in conjunction with dynamic contrast enhanced MRI [23] to accurately diagnose the hydronephrotic kidney.

## CONCLUSION

We applied sodium MRI to monitor non-invasively, in the intact rat kidney, distinct changes in the corticomedullary sodium profile under various physiologic and pathologic states. In all of these states the sodium profile was markedly different from that in the normal kidney, reflecting modulation in renal function. This methodology can be applied in humans and, in adjunct with the current ^{1}H imaging methods, improve the diagnosis and management of patients with renal failure.

## ACKNOWLEDGMENT

*Reprint requests to Prof. Hadassa Degani, Department of Biological Regulation, Weizmann Institute of Science, Rehovot 76100, Israel.*
*E-mail: hadassa.degani@weizmann.ac.il*

## REFERENCES

1. PUSCHETT JB: Pharmacological classification and renal actions of diuretics. *Cardiology* 84:4–13, 1994
2. BETTER OS, RUBINSTEIN I, WINAVER JM, KNOCHEL JP: Mannitol therapy revisited (1940–1997). *Kidney Int* 52:886–894, 1997
3. BUERKERT J, MARTIN D, PRASAD J, TRIGG D: Role of deep nephrons and the terminal collecting duct in a mannitol-induced diuresis. *Am J Physiol* 240:F411–422, 1981
4. GENNARI FJ, JOHNS C, CAFLISCH CR, CORTELL S: Dissociation of saline-induced natriuresis from urea washout in the rat. *Am J Physiol* 241:F250–256, 1981
5. KRAKUSIN JS, JENNINGS RB: Radioautographic localization of $^{22}$Na in the rat kidney. *A M A Arc Pathol* 59:471–486, 1955
6. MANITUS A, LEVITIN H, BECK D, EPSTEIN FH: On the mechanism of inpairment of renal concentrating ability in potassium deficiency. *J Clin Invest* 39:684–692, 1960
7. ATHERTON JC, HAI MA, THOMAS S: The time course of changes in renal tissue composition during mannitol diuresis in the rat. *J Physiol* 197:411–428, 1968
8. BENGELE HH, MATHIAS RS, PERKINS JH, ALEXANDER EA: Urinary concentrating defect in the aged rat. *Am J Physiol* 240:F147–150, 1981
9. WANG X, THOMAS SR, WEXLER AS: Outer medullary anatomy and the urine concentrating mechanism. *Am J Physiol* 274:F413–424, 1998
10. EDWARDS A, DELONG MJ, PALLONE TL: Interstitial water and solute recovery by inner medullary vasa recta. *Am J Physiol Renal Physiol* 278:F257–269, 2000
11. KNEPPER MA, SAIDEL GM, HASCALL VC, DWYER T: Concentration of solutes in the renal inner medulla: Interstitial hyaluronan as a mechano-osmotic transducer. *Am J Physiol Renal Physiol* 284:F433–446, 2003
12. CHRISTENSEN JD, BARRERE BJ, BOADA FE, *et al*: Quantitative tissue sodium concentration mapping of normal rat brain. *Magn Reson Med* 36:83–89, 1996
13. CONSTANTINIDES CD, KRAITCHMAN DL, O'BRIEN KO, *et al*: Noninvasive quantification of total sodium concentrations in acute reperfused myocardial infarction using $^{23}$Na MRI. *Magn Reson Med* 46:1144–1151, 2001
14. THULBORN KR, DAVIS D, ADAMS H, *et al*: Quantitative tissue sodium concentration mapping of the growth of focal cerebral tumors with sodium magnetic resonance imaging. *Magn Reson Med* 41:351–359, 1999
15. BANSAL N, SZCZEPANIAK L, TERNULLO D, *et al*: Effect of exercise on $^{23}$Na MRI and relaxation characteristics of the human calf muscle. *J Magn Reson Imaging* 11:532–538, 2000
16. CONSTANTINIDES CD, GILLEN JS, BOADA FE, *et al*: Human skeletal muscle: Sodium MR imaging and quantification-potential applications in exercise and disease. *Radiology* 216:559–568, 2000
17. MAEDA M, SEO Y, MURAKAMI M, *et al*: Sodium-23 MR imaging of the kidney in guinea pig at 2.1 T, following arterial, venous, and ureteral ligation. *Magn Reson Med* 16:361–367, 1990
18. RA JB, HILAL SK, OH CH, MUN IK: In vivo magnetic resonance imaging of sodium in the human body. *Magn Reson Med* 7:11–22, 1988
19. BOGUSKY RT, GARWOOD M, MATSON GB, *et al*: Localization of phosphorus metabolites and sodium ions in the rat kidney. *Magn Reson Med* 3:251–261, 1986
20. BANSAL N, SESHAN V: Three-dimensional triple quantum-filtered 23Na imaging of rabbit kidney with weighted signal averaging. *J Magn Reson Imaging* 5:761–767, 1995
21. WOLFF SD, ENG C, BALABAN RS: NMR studies of renal phosphate metabolites in vivo: Effects of hydration and dehydration. *Am J Physiol* 255:F581–589, 1988
22. WOLFF SD, ENG J, BERKOWITZ BA, *et al*: Sodium-23 nuclear magnetic resonance imaging of the rabbit kidney in vivo. *Am J Physiol* 258:F1125–1131, 1990
23. WEN JG, CHEN Y, RINGGAARD S, *et al*: Evaluation of renal function in normal and hydronephrotic kidneys in rats using gadolinium diethylenetetramine-pentaacetic acid enhanced dynamic magnetic resonance imaging. *J Urol* 163:1264–1270, 2000
24. UGURBIL K, GARWOOD M, RATH AR: Optimization of modulation functions to improve insensitivity of adiabatic pulses to variation in B1 magnitude. *J Magn Reson* 80:448–469, 1988
25. BOULANGER Y, VINAY P: Nuclear magnetic resonance monitoring of sodium in biological tissues. *Can J Physiol Pharmacol* 67:820–828, 1989
26. BOADA FE, CHRISTENSEN JD, HUANG-HELLINGER FR, *et al*: Quantitative in vivo tissue sodium concentration maps: The effects of biexponential relaxation. *Magn Reson Med* 32:219–223, 1994
27. FORSEN S, LINDMAN B: Ion binding in biological systems as studied by NMR spectroscopy. *Methods Biochem Anal* 27:289–486, 1981
28. ELLISON DH, VELAZQUEZ H, WRIGHT FS: Adaptation of the distal convoluted tubule of the rat. Structural and functional effects of dietary salt intake and chronic diuretic infusion. *J Clin Invest* 83:113–126, 1989
29. SZENASI G, BENCSATH P, TAKACS L: Proximal tubular transport and urinary excretion of sodium after renal denervation in sodium depleted rats. *Pflugers Arch* 403:146–150, 1985
30. LOTE CJ: *Principles of Renal Physiology*, London, Chapman & Hall, 1994
31. HERVY S, THOMAS SR: Inner medullary lactate production and urine-concentrating mechanism: A flat medullary model. *Am J Physiol Renal Physiol* 284:F65–81, 2003
32. VALTIN H: Sequestration of urea and nonurea solutes in renal tissues of rats with hereditary hypothalamic diabetes insipidus: Effect of vasopressin and dehydration on the countercurrent mechanism. *J Clin Invest* 45:337–345, 1966
33. FRASER AG, COWIE JF, LAMBIE AT, ROBSON JS: The effects of furosemide on the osmolality of the urine and the composition of renal tissue. *J Pharmacol Exp Ther* 158:475–486, 1967
34. AZAR S, TOBIAN L, ISHII M: Prolonged water diuresis affecting solutes and interstitial cells of renal papilla. *Am J Physiol* 221:75–79, 1971
35. WALD H, SCHERZER P, POPOVTZER MM: Inhibition of thick ascending limb Na+-K+-ATPase activity in salt-loaded rats by furosemide. *Am J Physiol* 256:F549–555, 1989
36. JAMISON RL, KRIZ W: *Urinary Concentrating Mechanism*, New York, Oxford, Oxford University Press, Inc., 1982
37. LAW RO: The volume and ionic composition of cells in incubated slices of rat renal cortex, medulla and papilla. *Biochim Biophys Acta* 931:276–285, 1987

38. Jones B, Simpson DP: Intracellular pH in intact rat renal cortex estimated with [14C]-5, 5-dimethyl-2, 4-oxazolidinedione. *Ren Physiol* 6:19–27, 1983

39. Gottschalk CW, Mylle M: Micropuncture study of the mammalian urinary concentrating mechanism: Evidence for the countercurrent hypothesis. 1959. *J Am Soc Nephrol* 8:153–164; discussion 153–159, 1997

40. Jamison RL: The renal concentrating mechanism: Micropuncture studies of the renal medulla. *Fed Proc* 42:2392–2397, 1983

41. Koepsell H, Nicholson WA, Kriz W, Hohling HJ: Measurements of exponential gradients of sodium and chlorine in the rat kidney medulla using the electron microprobe. *Pflugers Arch* 350:167–184, 1974

42. Martinez-Maldonado M, Eknoyan G, Suki WN: Influence of volume expansion on renal diluting capacity in the rat. *Clin Sci Mol Med* 46:331–345, 1974

43. Pallone TL, Yagil Y, Jamison RL: Effect of small-solute gradients on transcapillary fluid movement in renal inner medulla. *Am J Physiol* 257:F547–553, 1989

44. Hargitay B, Kuhn W: The multiplication principle as the basis for concentrating urine in the kidney. *J Am Soc Nephrol* 12:1566–1586, 2001

45. Knepper MA: Measurement of osmolality in kidney slices using vapor pressure osmometry. *Kidney Int* 21:653–655, 1982

46. Thomas SR: Cycles and separations in a model of the renal medulla. *Am J Physiol* 275:F671–690, 1998

47. Greger R: New insights into the molecular mechanism of the action of diuretics. *Nephrol Dial Transplant* 14:536–540, 1999

48. Greger R: Physiology of renal sodium transport. *Am J Med Sci* 319:51–62, 2000

49. Romano G, Favret G, Federico E, Bartoli E: The site of action of furosemide. *Pharmacol Res* 37:409–419, 1998

50. Sekine T, Watanabe N, Hosoyamada M, *et al*: Expression cloning and characterization of a novel multispecific organic anion transporter. *J Biol Chem* 272:18526–18529, 1997

51. Greger R: How does the macula densa sense tubule function? *Nephrol Dial Transplant* 12:2215–2217, 1997

52. Mostbeck GH, Zontsich T, Turetschek K: Ultrasound of the kidney: Obstruction and medical diseases. *Eur Radiol* 11:1878–1889, 2001

53. Nolte-Ernsting CC, Adam GB, Gunther RW: MR urography: Examination techniques and clinical applications. *Eur Radiol* 11(3):355–72:355–372, 2001

54. O'Malley ME, Soto JA, Yucel EK: MR urography: Evaluation of a three-dimensional fast spin-echo technique in patients with hydronephrosis. *AJR Am J Roentgenol* 168:387–392, 1997

55. Wen JG: Partial unilateral ureteral obstruction in rats. *Neurourol Urodyn* 21:231–250, 2002